THIRTEENTH EUROPEAN ROTORCRAFT FORUM

7-1
Paper No. 1

NUMERICAL SIMULATIONS OF DYNAMIC RESPONSE OF FIXED AND ROTARY WING AIRCRAFT TO A LARGE AIRPLANE WAKE

Shigeru SAITO

NATIONAL AEROSPACE LABORATORY
7-44-1, JINDAIJIHIGASHI-MACHI,
CHOFU, TOKYO, 182 JAPAN

Akira AZUMA, Yoshinori OKUNO and Tomohiko HASEGAWA

INSTITUTE OF INTERDISCIPLINARY RESEARCH
FACULTY OF ENGINEERING, THE UNIVERSITY OF TOKYO
4-6-1, KOMABA, MEGURO-KU,
TOKYO, 153 JAPAN

September 8-11, 1987

ARLES, FRANCE

ASSOCIATION AERONAUTIQUE ET ASTRONAUTIQUE DE FRANCE

NUMERICAL SIMULATIONS OF DYNAMIC RESPONSE OF FIXED AND ROTARY WING AIRCRAFT TO A LARGE AIRPLANE WAKE

Shigeru SAITO

National Aerospace Laboratory
Tokyo, Japan

Akira AZUMA, Yoshinori OKUNO
and
Tomohiko HASEGAWA

The University of Tokyo
Tokyo, Japan

ABSTRACT

Numerical simulations of aircraft flight dynamics are performed in order to investigate the dynamic characteristics of fixed and rotary wing aircraft penetrating a pair of trailing vortices of a preceding large airplane such as jumbo jet airplane. The aerodynamic forces acting on main wing or rotary wing, which are fully coupled with the body motion of the aircraft in six-degrees of freedom are calculated by using the Local Circulation Method (LCM) [1] for the fixed wing and the Local Momentum Theory (LMT) [2] for the rotary wing.

Time histories of the dynamic behavior of two airplanes and a helicopter are presented for various parameters such as separation distance between the preceding airplane and the penetrating aircraft, mass and span or rotor radius of aircraft, and flight path angle with respect to the tip vortices of the preceding airplane.

The dynamic response of airplane is much severer than that of helicopter. Specifically, the rolling response of the penetrating airplane flying along the vortex core with negative path angle γ is disturbed by the induced velocity generated by the vortex core with the maximum value of 110 degrees when it just hits a margin of the core. However, in the case of positive γ, for example γ = 2 degrees, the penetrating airplane is disturbed before it approaches to the vortex core and kicked out by the induced velocity around the core, and thus the response is more mild than that of the helicopter in the equivalent flight condition in which the helicopter penetrates the core itself.

1. INTRODUCTION

In airport environments, an aircraft has some high possibility to penetrate a trail of tip vortices of large jet airplane just after the taking-off or landing. Severe wake vortices generated by the large airplane can induce a sudden roll excursion or roll upset of the aircraft and often be cause of structural damage. To avoid these hazardous wake vortices, the Federal Aviation Administration (FAA) requires 11 km (6 naut. mi.) spacing for a small business jet under 5.7 ton (12,500 lb) behind a large wide-body jet, 9 km (5 naut. mi.) for a larger transport under 136 ton (300,000 lb) and 7.4 km (4 naut. mi.) for a wide-body transport behind another same category [3]. Even at the high altitude, an airplane has sometimes hazardous experience due to large vortices generated in a special atomospheric condition like a tornado [4].

Many research works about the tip vortices of airplane were reported and many theoretical models of the vortices including the effects of viscosity were presented, for example in references [5]~[7]. A lots of flight tests were conducted to measure the velocity field of the wake vortices in flight and the dynamic behavior of airplane penetrating the wake vortices [8]~[16]. Studies of the dynamic response of helicopter penetrating the tip vortices, on the other hand, were reported only a few papers [17]~[22]. Flight test data for the helicopter were also limited. Parameters which may give some influence on the dynamic behavior of the aircraft are air density, ρ, mass ratio, m/m_A, span or rotor radius ratio, b/b_A or R/b_A, speed ratio, U/U_A, nondimensional separation distance, x/b_A, y/b_A, z/b_A, flight path angles γ, and flight course angle Ψ_W.

The purpose of this paper is to analyze the dynamic responses of two airplanes and a helicopter in six-degrees of freedom, which penetrate a pair of trailing vortices generated by a large preceding airplane, and to compare the results between the airplane and the helicopter. Time histories of the dynamic response such as vertical acceleration, angles and angular rates of attitude, load factor and so on, are presented. The dynamic behaviors of the penetrating airplane and helicopter are depicted graphically to understand their phenomena.

2. GEOMETRY OF A TRAILING VORTEX

A sheet of trailing vortices wake system generated by a conventional lifting wing of moderate sweep and aspect ratio is unstable and tends to roll-up to a pair of oppositely rotating trailing vortices, as shown in Figure 1. In this section, the mathematical model of the pair of trailing vortices is described. Under assumptions that the flow is steady, axisymmetric, laminar and incompressible, and the Reynolds number of the main flow, $U_A x/\nu$, where x is the axial distance, is large, the axial velocity q_x, radial

velocity q_r, rotational velocity q_θ can be given by solving the Navier-Stokes' equations as follows [3],[21]~[23]:

$$\Gamma = \Gamma_0\sqrt{1-(2y/b_A)^2} \tag{1}$$

$$\left.\begin{aligned} q_x &= (D_0/4\pi\rho\nu_e x)\exp(-(U_A r2/4\nu_e x)) = -q_x^*\exp(-r/r^*)^2 \\ q_r &= -(rD_0/8\pi\rho\nu_e x2)\exp(-(U_A r2/4\nu_e x)) = -q_r^*\exp(-r/r^*)^2 \\ q_\theta &= (\Gamma_0/2\pi r)\exp\{1-\exp((U_A r^2/4\nu_e x)) = q_\theta^*(r^*/r)\{\exp(-r/r^*)^2\} \end{aligned}\right\} (2)$$

where

$$\left.\begin{aligned} \Gamma_0 &= \Gamma(y=0) = (4L/\pi\rho b_A U_A) \\ q_x^* &= D_0/4\pi\rho\nu_e x \\ q_r^* &= (rD_0/2\pi\rho U_A x)/r*2 \\ q_\theta^* &= (\Gamma_0/4\pi x)\sqrt{U_A x/\nu_e} = (\Gamma_0/4\pi)\sqrt{U_A/\nu_e}\,/\sqrt{x} \\ r^* &= 2x/\sqrt{U_A x/\nu_e} = (2/\sqrt{U_A x/\nu_e})\sqrt{x} \\ D_0 &= 2\pi\int_0^\infty \rho(U_A-u)urdr = 2\pi\int_0^\infty \rho U_A urdr, \end{aligned}\right\} (3)$$

and where D_0 and ν_e are the profile drag and the "effective eddy viscosity" rather than the kinematic viscosity respectively [13]. The value of ν_e is given by

$$\nu_e = \nu + a\Gamma_0 \tag{4}$$

where "a" is an empirical constant, whose precise value is very difficult to define but is in the range 10^{-3} to 10^{-4} such as a = 0.0002 [10] ~ 0.002 [19]. In this analysis, the trailing vortices are assumed to be frozen.

In order to check the validity of the theoretical model of the trailing vortex wake system, comparisons of the calculated results with flight test measurements are made as shown in Figure 2. In this figure, three velocity components of the tip vortices are shown at two different separation distances from a large airplane (in this case, Boeing 747)[8]. At distance of x=10,500 m, the correlation between three velocity components and flight test measurements are very good, even though the penetrating airplane was influenced by the tip vortices itself. On the other hand, at distance of x=24,000 m, data of velocity components given by flight test show quite different features compared with calculated results. In the theoretical calculation, instability of the vortex core or atomospheric conditions were not taken into account. Therefore features of the velocity components at any separation distance remain same. From this comparison it must be considered that over the range of 20,000 m theoretical results do not simulate the actual flow field of the tip vortices. In this study, range of the separation distance were limited till 20,000 m.

3. MODEL AIRPLANES AND A HELICOPTER AND THEIR FLIGHT CONDITIONS

Two types of fixed-wing aircraft (airplanes of model A and model B) and one type of hingeless-rotor helicopter are chosen to investigate the dynamic responses when penetrating a pair of tip vortices generated by a large preceding airplane. The dimensions of the preceding airplane and the penetrating aircraft are listed in Table 1 and Table 2 respectively. Every flight are directed to hit the center of one of vortex core at any given initial conditions as shown in Figure 1. Since both the preceding airplane and the penetrating aircraft are moving forward with their own flight velocities, U_A and U_P (U_H for a rotary wing aircraft) respectively, the distance of the penetrating aircraft behind the preceding airplane is more than x_0 when the center of gravity of the latter aircraft just hits the vortex core center.

The spatial CG position of the penetrating aircraft with respect to the preceding airplane frame (X,Y,Z) is given by

$$\begin{Bmatrix} X_{CG} \\ Y_{CG} \\ Z_{CG} \end{Bmatrix} = \begin{Bmatrix} X_{CG,0} \\ Y_{CG,0} \\ Z_{CG,0} \end{Bmatrix} + \begin{Bmatrix} U_A t \\ 0 \\ 0 \end{Bmatrix} + \int_0^t T_2 \cdot T_1 \cdot \begin{Bmatrix} U_{X_B} \\ U_{Y_B} \\ U_{Z_B} \end{Bmatrix} dt \qquad (5)$$

where T_1 and T_2 are transformation matrices from the body frame

(X_B, Y_B, Z_B) of the penetrating aircraft to the initial body frame $(X_{B,0}, Y_{B,0}, Z_{B,0})$ which is the body frame at time t = 0, and from the initial body frame to the generating aircraft frame (X,Y,Z), respectively.

$$T_1 = \begin{bmatrix} \cos\Theta\cos\Psi & \sin\Phi\sin\Theta\cos\Psi-\cos\Phi\sin\Psi & \cos\Phi\sin\Theta\cos\Psi+\sin\Phi\sin\Psi \\ \cos\Theta\sin\Psi & \sin\Phi\sin\Theta\sin\Psi+\cos\Phi\cos\Psi & \cos\Phi\sin\Theta\sin\Psi-\sin\Phi\cos\Psi \\ -\sin\Theta & \sin\Phi\cos\Theta & \cos\Phi\cos\Theta \end{bmatrix} \quad (6)$$

$$T_2 = \begin{bmatrix} \cos\Theta_0\Psi_0 & \cos\Theta_0\Psi_0 & -\sin\Theta_0 \\ \sin\Phi_0\sin\Theta_0\cos\Psi_0-\cos\Phi_0\sin\Psi_0 & \sin\Phi_0\sin\Theta_0\sin\Psi_0+\cos\Phi_0\cos\Psi_0 & \cos\Theta_0\sin\Phi_0 \\ \cos\Phi_0\sin\Theta_0\cos\Psi_0+\sin\Phi_0\sin\Psi_0 & \cos\Phi_0\sin\Theta_0\sin\Psi_0-\sin\Phi_0\cos\Psi_0 & \cos\Phi_0\cos\Theta_0 \end{bmatrix} \quad (7)$$

and where $(\Phi_0, \Theta_0, \Psi_0)$ are the initial setting angles of the body frame with respect to the (X,Y,Z) frame.

Then the relative position of the CG of the aircraft or the rotor hub with respect to the vortex core frame (x,y,z), the origin is fixed to the respect wing tip, is given as follows:

$$\begin{Bmatrix} x \\ y \\ z \end{Bmatrix} = \begin{Bmatrix} X_{CG} \\ Y_{CG} \\ Z_{CG} \end{Bmatrix} + T_1 \cdot T_2 \begin{Bmatrix} l_R \\ 0 \\ h_R \end{Bmatrix} - \begin{Bmatrix} 0 \\ \pm b_A \\ 0 \end{Bmatrix} \quad (8)$$

where $(l_R, 0, h_R)^T$ is the hub position with respect to the body frame and $\pm$ gives the left and right trailing vortices respectively.

Various flight conditions of the preceding airplane and the penetrating aircraft are given in Table 3.

4. EQUATIONS OF MOTION OF THE FIXED AND ROTARY WING AIRCRAFT

By referring to Figure 3, equations of motion of the penetrating aircraft in six-degrees of freedom can be given by

$$\left.\begin{aligned} m(\dot{u}+qw-rv) &= F_{X_B} \\ m(\dot{v}+ru-pw) &= F_{Y_B} \\ m(\dot{w}+pv-qu) &= F_{Z_B} \end{aligned}\right\} \quad (9)$$

$$\left.\begin{aligned} \dot{p}I_{X_B}+(rp-\dot{q})J_{X_BY_B}-(\dot{r}+pq)J_{Z_BX_B}+(r^2-q^2)J_{Y_BZ_B}+qr(I_{Z_B}-I_{Y_B}) &= M_{X_B} \\ \dot{q}I_{Y_B}+(pq-\dot{r})J_{Y_BZ_B}-(\dot{p}+qr)J_{X_BY_B}+(p^2-r^2)J_{Z_BX_B}+rp(I_{X_B}-I_{Z_B}) &= M_{Y_B} \\ \dot{r}I_{Z_B}+(qr-\dot{p})J_{Z_BX_B}-(\dot{q}+rp)J_{Y_BZ_B}+(q^2-p^2)J_{X_BY_B}+pq(I_{Y_B}-I_{X_B}) &= M_{Z_B} \end{aligned}\right\} \quad (10)$$

where the mass (m), the moments of inertia ($I_{X_B}, I_{Y_B}, I_{Z_B}$) and the product of inertia ($J_{X_BZ_B}$) are those related to the penetrating aircraft body. In equations (9) and (10), the body of aircraft is assumed to have a symmetric configuration. Therefore the products of inertia about X_B-Y_B axis and Y_B-X_B axis become zero ($J_{X_BY_B}=J_{Y_BZ_B}=0$). The external forces ($F_{X_B}, F_{Y_B}, F_{Z_B}$) and moments ($M_{X_B}, M_{Y_B}, M_{Z_B}$) are given from fixed wing or rotary wing, horizontal and vertical wings, and fuselage. The aerodynamic forces and moments acting on either the main wing or rotary wing are calculated by the LCM or the LMT in which the spanwise steps is performed by $\Delta x = \eta/b_A$ or $r/R = 1/20$.

In the LCM and LMT, the induced velocity generated by the fixed or rotary wing at any spanwise position is determined by using the quasi-lifting surface theory [1] and lifting line theory [2] respectively, and three dimensional gust velocities which are spread spatially are easily introduced in these methods as same as references [21]~[23]. For fuselage, tail rotor, vertical and horizontal wing of the aircraft, the aerodynamic properties are calculated for simplicity by using the experimental data without the usage of these methods.

The body motion, in the six-degrees of freedom, of the penetrating aircraft is calculated by the Runge-Kutta method. The timewise increment of the computation is 1/100 second for the airplane and $2\pi/360\Omega$ second for the helicopter.

5. NUMERICAL SIMULATIONS

In this section, results of the dynamic response of a penetrating aircraft are presented and discussed. After getting a trimmed condition for a given flight path angle γ, the penetrating aircraft starts to fly to be directed to the center of vortex core from a specified initial position.

Figures 4 (a) and (b) schematically show typical examples of flight trajectories of the airplane and hilicopter in side view, top view and back view respectively.

Figure 5 shows a comparison between a calculated result based on the present method and a flight test of an airplane. In this case, the preceding airplane was the Convair 990 and the penetrating aircraft was the Cessna 210 [13]. The penetrating aircraft was controlled in order to hit the vortex core at separation distance x=5,180 m. The calculated results with respect to the longitudinal motion are in good correlation with the experimental data. However, in the lateral motion, the calculated results do not agree with the experimental data. This discrepancy might be resulted from some differences in the control inputs (aileron and rudder).

In the following subsections, the dynamic response of the penetrating aircraft are investigated for the model A, the model B and tha hingeless-rotor helicopter for various flight conditions with different parameters such as separation distance x, flight path angle γ and flight course angle Ψ_W.

5-1. Effects of the separation distance (x)

The separation distance between the penetrating aircraft and the preceding airplane is one of the important parameters in the dynamic response of the aircraft. Figures 6 (a), (b) and (c) show maximum attitudes, maximum angular velocities, and maximum accelerations of the penetrating aircraft (model A) respectively. The flight path angle and the flight course angle were assumed to be γ=0 degree and Ψ_W=90 degrees respectively. The separation distances were

taken from x=5,000 m to x=20,000 m. The attitudes of the penetrating aircraft were not changed against the separation distance (x). However, the pitch angular velocity (q) attains over 30 deg/sec at separation distance of x=5,000 m. As the separation distance increases, this angular velocity decrease gradually. On the other hand, the vertical acceleration, as shown in Figure 6 (c), exceeds 2g within $x < 18{,}000$ m. This is resulted from strong up- and down-wash caused by the tip vortices.

Similar calculations were performed for the model B airplane which had larger gross weight and wing span than those of the model A. The results are shown in Figure 7 (a), (b) and (c). The flight attitudes did not change so much like the case of the model A. In the angular velocities, the pitch rate is smaller than that of model A (less than 10 deg/sec). Besides, the vertical acceleration of

model B is less than 2g over the whole range investigated.

Shown in Figures 8 (a), (b) and (c) are calculated results for the response of the hingeless-rotor helicopter. In Comparison with the results of the airplanes, the trend of the maximum attitudes is almost same as that of the model A. Different from the airplanes (model A and B), the roll rate in the angular velocities is predominant.

5-2. Effects of the flight path angle (γ)

Effects of the flight path angle (γ) on the dynamic response of the penetrating aircraft, the model airplane, A and B, and the helicopter, are investigated. An initial vertical position (z) was taken at z=15 m for positive γ and z=-15 m for negative γ as shown in Figure 9 (a) and (b). Within $|\gamma|$=2 degrees, the calculation was omitted because the initial position is located inside of the vortex core. Shown in Figure 10, 11 and 12 respectively are (a) the maximum attitudes, (b) maximum angular velocities and (c) maximum accelerations. Compared with the perpendicular penetration, the penetrating aircraft were drastically influenced by the flow field of the tip vortices. Specifically the response in roll angle and the roll rate is very significant for three aircraft. For the model A, the rolling attitude exceeds 110 degrees at x=5,000 m. On the other hand, maximum value of the model B shows a more mild than that of the model A. The trend of the response is also quite different from that of the model A. For the positive γ the model B responds much severer than the model A, whereas for the negative γ, the situation is reversed. For the accelerations about the respective body axes, both the model A and the model B get the 2g acceleration in the z axis, whereas the helicopter has small amount of the acceleration about 1.5g. As the separation distance increases, the magnitude of these accelerations tends to decrease. For the helicopter, the dynamic response is very mild and the magnitude of the highest value in the pitch response is less than 40 degrees.

Shown in Figure 13 are flight trajectories viewed from the rear side of three types of the penetrating aircraft. Since the flight velocity of the model A is less than that of the model B, the former is kicked out from the core before it reaches the core center. As results, the model A rolls severely with negative bank angle.

5-3. Effects of the flight course angle (Ψ_W)

In this case, as shown in Figure 14, the penetrating aircraft is directed to hit the center of vortex core with the flight path angle of γ=5 degrees and the separation distance of x=5,000 m. Figure 15, 16 and 17 show the effects of the flight course Ψ_W on the dynamic response of airplanes, the model A and model B and the helicopter. As the Ψ_W decreases or the flight course approaches to be parallel to the tip vortex, the roll response increases for all

three types of aircraft. At Ψ_W=0 degree, the magnitude of the body attitudes decreases only for the model A. This is because the model A is kicked out by the tip vortex as shown in Figure 18 (a), (b) and (c).

Finally the minimum distance between the CG position of the penetrating airplane or the center of hub of the helicopter and the core of the tip vortex is shown in Figure 19 (a), (b) and (c). As shown in (a), the every penetrating aircraft pass through inside of the vortex core. In (b) and (c) the model A is often kicked out by the tip vortex because of the roll upset, whereas the helicopter can penetrate the vortex core.

6. CONCLUSIONS AND RECOMMENDATIONS

The Local Circulation Method (LCM) and the Local Momentum Theory (LMT) have been applied to analyze the dynamic responses of the fixed wing and rotary wing aircraft in six-degrees of freedom respectively, which penetrate a pair of trailing vortices of a preceding large airplane. Parametric studies have been performed to investigate important parameters which may influence on the dynamic response of the penetrating aircraft. The major results in this theoretical study are drawn as follows:

(1) There is good correlation between the simulated data of flow field by a pair of tip vortices and the experimental measured data in flight.

(2) For the penetrating airplanes, the dynamic response becomes large as the flight course angle (Ψ_W) approaches to zero (parallel penetration).

(3) For the penetrating helicopter, the dynamic response, which is coupled with the longitudinal and lateral motion, is generally mild in comparison with the results of the airplanes.

(4) The minimum distance between the penetrating aircraft and the core center of the vortex depends on the individual flight condition for all types of the aircraft. The small airplane is often kicked out by the tip vortex even though it is directed to hit the center of the vortex core.

In the present work, two types of airplanes and a helicopter were used to investigate the dynamic response when they penetrate the trailing vortices generated by a preceding large airplane. Although the calculations were performed in limited cases, they are many combinations of other types of airplane and helicopters and their flight conditions with respect to the trailing vortices of the preceding airplane. Furthermore, the flight configuration of the preceding airplane may be altered in the future calculations.

7. REFERENCES

1. Azuma, A., Nasu, K. and Hayashi, T.: An Extension of the Local Momentum Theory to Rotors Operating in a Twisted Flow Field, Vertica , Vol.7, No.1, PP.45-59, 1983.

2. Azuma, A. and Kawachi, K.: Local Momentum Theory and Its Application to the Rotary Wing, J. of Aircraft, Vol.16, No.1, 1979, also AIAA Paper 75-865.

3. Klass, P.J.: Wake Vortex Sensing Efforts Advance, Aviation Week Space Technology, PP.92-99, April 25, 1977.

4. Parks, E.K., Wingrove, R.C., Bach, R.E. and Metha, R.S.: Identification of Vortex-Induced Clear Air Turbulence Using Airline Flight Rewards. J. of Aircraft, Vol.22, No.2, 1985.

5. Lamb, H.: Hydrodynamics, Fifth Edition, 1930.

6. McCormick, B.W., Tangler, J.L. and Sherrieb, H.E.: Structure of Trailing Vortices, J. of Aircraft, Vol.5, No.3, pp.260-267, 1968.

7. Lee, H. and Schetz, J.A.: Experimental Results for Reynolds Number Effects on Trailing Vortices, J. of Aircraft, Vol.22, No.3, 1985.

8. Verstynen, H.A., Jr. and Dunhum, R,E., Jr.: A Flight Investigation of the Trailing Vortices Generating by a Jumbo Jet Transport, NASA TN D-7172.

9. Kerr, T.H. and Dee, F.W.: A flight Investigation into the persistence of Trailing Vortices behind Large Aircraft, British A.R.C., C.P.489, 1959.

10. Rose, R. and Dee, F.W.: Aircraft Vortex Wakes and their Efforts on Aircraft, British A.R.C., C.P.795, 1965.

11. Sammonds, R.I. and Stinnett, G.W., Jr. and Larsen, W.E.: Hazard Criteria for Wake Vortex Encounters, AIAA 3rd Atomospheric Flight Mechanics Conference, June 7-9, 1976.

12. McGowan, W.A.: Calculated Normal Load Factors on Light Airplanes Traversing the Trailing Vortices of Heavy Transport Airplane, NASA TN D-829.

13. Wetmore, J.W. and Reeder, J.P.: Aircraft Vortex Wakes in Relation to Terminal Operations, NASA TN D-1777.

14. Andrews, W.H., Robinson, G.H. and Larson, R.R.: Exploratory Flight Investigation of Aircraft Response to the Wing Vortex Wake Generated by Jet Transport Aircraft. NASA TN D-6655.

15. Robinson, G.H. and Larson, R.R.: A Flight Evaluation of Methods for Predicting Vortex Wake Effects on Trailing Aircraft, NASA TN D-6904.

16. Nelson, R.C. and McCormick, B.W.: The Dynamic Behavior of an Aircraft Encountering Aircraft Wake Turbulence.

17. Dunham, R.E., Jr., Holbrook, G.T., Mantay, W.R. Campbell, R.L. and Van Gunst, R.W.: Flight-Test Experience of a Helicopter Encountering an Airplane Trailing Vortex, 32nd Annual National V/STOL Forum of the AHS, No.1063, 1976.

18. Mantay, W.R., Holbrook, G.T., Campbell, R.L. and Tomaine, R.L.: Flight Investigation of the Response of a Helicopter to the Trailing Vortex of a Fixed-wing Aircraft, AIAA 3rd Atomospheric Fluid Mechanics Conference, 1976.

19. Dreier, M.E.: The Influence of a Trailing Tip Vortex on a Thrusting Rotor, A Thesis in Aerospace Engineering, The Pennsylvania State University, 1977.

20. Curtiss, H.C., Jr. and Zhou, Zheng-gen: The Dynamic Response of Helicopters to Fixed Wing Aircraft, Theoretical Basis of Helicopter Technology, Seminar at Nanjing Aeronautical University, Nanjing 1985.

21. Azuma, A., Kawachi, K. and Saito, S.: The Local Momentum Method and Its Application to Helicopter Aero- and Flight-Dynamics, Theoretical Basis of Helicopter Technology, Seminar at Nanjing Aeronautical University, Nanjing, 1985.

22. Azuma, A., Saito, S. and Kawachi, K.: Response of Helicopter penetrating the Tip Vortices of Large Airplane, Vertica, Vol.11, No.1/2, pp.65-76, 1987.

23. Saito, S., Azuma, A., Kawachi, K. and Okuno, Y.: Study of the Dynamic Response of Helicopters to a Large Airplane, Twelfth European Rotorcraft Forum, Garmisch-Partenkirchen, FRG, Sept. 22-25, 1986.

NOMENCLATURE

a	empirical constant of effective eddy viscosity
$(a_{X_B}, a_{Y_B}, a_{Z_B})$	acceleration of aircraft about body axis
b	wing span of airplane
D_0	profile drag of aircraft
D_{min}	minimum distance between the penetrating aircraft and the vortex core center
(F_{XB}, F_{YB}, F_{ZB})	external forces given by eq.(7)
g	acceleration of gravity
$(I_{X_B}, I_{Y_B}, I_{Z_B})$	moments of inertia of aircraft
$J_{X_BZ_B}$	product of inertia of aircraft

L	lift
(l_H, h_H)	position of horizontal wing from CG position
(l_R, h_R)	position of hub center from CG position
(l_V, h_V)	position of vertical wing from CG position
$(M_{X_B}, M_{Y_B}, M_{Z_B})$	external moments given by eq.(8)
m	mass of aircraft
(p,q,r)	angular velocity of body
(q_x, q_y, q_z)	longitudinal, radial and circumferential gust components shown in Fig. 1
(q_x^*, q_y^*, q_z^*)	longitudinal, radial and circumferential gust components at core center
R	rotor radius
r	radial position or distance from the center of vortex core
r^*	radius of tip vortex core
S	wing area or rotor disk area
T_1, T_2	transformation matrix
t	time
U	flight speed of aircraft
(u,v,w)	gust velocity components shown in Fig. 1
(X,Y,Z)	coordinate system fixed to airplane shown in Fig. 1
(X_B, Y_B, Z_B)	coordinate system fixed to helicopter shown in Fig. 1
(X_{CG}, Y_{CG}, Z_{CG})	longitudinal, lateral and vertical position of helicopter center of gravity in (X,Y,Z) coordinate system
(x,y,z)	coordinate system fixed to wing tip shown in Fig. 1
x	nondimensional radial position = r/R, or separation distance
(x_{CG}, y_{CG}, z_{CG})	longitudinal, lateral and vertical position of helicopter center of gravity in (x,y,z) coordinate system
y	spanwise position
α	angle of attack
Γ	circulation
Γ_0	circulation of aircraft at midspan
γ	flight path angle of a penetrating aircraft
Δ	small increment
η	efficiency or spanwise position
(Φ, Θ, Ψ)	attitudes of a penetrating aircraft
$(\Phi_0, \Theta_0, \Psi_0)$	initial setting angle of body frame
μ	advance ratio = $U/R\Omega$
ν	kinematic viscosity
ν_e	effective eddy viscosity
ρ	air density
Ψ_W	flight course angle of a penetrating aircraft with respect to wake
Ω	rotor rotational speed

Subscripts:

$( )_A$ quantity concerning with a preceding airplane

$( )_H$ quantity concerning with helicopter

$( )_P$ quantity concerning with a penetrating airplane

$\dot{( )}$ time derivation

Table 1. Dimensions of a preceding airplane.

Items	Dimensions
Wing span b_A (m)	59.6
Wing area S_A (m^2)	511.0
Flight speed U_A (m/s)	94.4
Mass m_A (Kg)	2.11×10^5

Table 2. Dimensions of three types of aircraft.

Items		Airplanes		Helicopter
		Model A	Model B	
Gross mass	m (kg)	980.0	28,557.2	2,850.0
Moment of inertia of body	I_X (kgm^2)	1,460.0	80,8500.0	2,380.0
Moment of inertia of body	I_Y (kgm^2)	1,770.0	539,000.0	7,314.0
Moment of inertia of body	I_Z (kgm^2)	3,070.0	1,342,600.0	5,560.0
Product of inertia	J_{XZ} (kgm^2)	778.5	0.0	1,057.0
For Main Wing				
Span	b (m)	9.42	30.5	---
Mean aerodynamic chord	c (m)	1.525	3.205	---
Wing area	S_m (m^2)	14.0	92.9	---
Aspect ratio	AR	6.34	10.0	---
Sweep angle	Λ (deg)	0.0	0.0	---
Dihedral angle	Γ (deg)	7.0	5.0	---
Setting angle	i_w (deg)	2.5	0.0	---
For Main Rotor		---	---	See Ref.23
For Tail Rotor		---	---	See Ref.23
For Horizontal Wing				
Wing area	S_H (m^2)	3.32	21.5	1.0
Span	bH (m)	3.47	10.51	2.5
Chord	c_H (m)	1.03	1.97	0.4
Aspect ratio	AR_H	3.62	5.0	6.25
Position	(l_H, h_H)	(4.07, 0.0)	(11.88, 0.0)	(5.06, 0.617)
Efficiency	η	0.8	0.8	0.7
For Vertical Wing				
Wing area	S_v (m^2)	1.5	16.72	2.24
Span	b_v (m)	1.7	4.9	1.28
Chord	c_v (m)	1.1	3.07	1.75
Aspect ratio	AR_v	1.93	1.44	5.73
Position	(l_v, h_v)	(44.6, 0.45)	(10.79, 3.77)	(5.27, 0.219)
Efficiency	η	0.8	0.8	0.8

Table 3. Flight conditions of the penetrating aircraft with respect to the preceding airplane.

Aircraft		Figs	m_t/m_0	$2R/b_0$ or b/b_0	U/U_0	$(x_0/b_0, y_0/b_0, z_0/b_0)$	Ψ_u(deg)	γ(deg)	Flight
Airplanes	Model A	7-(a)	0.0047	0.158	0.597	(167.78, 3.86, 0)	90	0	Level
		12-(a)	0.0047	0.158	0.597	(170.69, 2.18,-0.29)	30	5	Climb
		17-(a)	0.0047	0.158	0.597	(167.78, 0.5, -0.25)	0	4	Climb
	Model B	7-(a)	0.135	0.512	0.8	(167.78, 3.86, 0)	90	0	Level
		12-(a)	0.135	0.512	0.8	(170.69, 2.18,-0.29)	30	5	Climb
		17-(a)	0.135	0.512	0.8	(167.78, 0.5, -0.25)	0	4	Climb
Helicopter		7-(a)	0.0135	0.185	0.468	(167.78, 1.34, 0)	90	0	Level
		12-(a)	0.0135	0.185	0.468	(170.69, 1.08,-0.14)	30	5	Climb
		17-(a)	0.0135	0.185	0.468	(167.78, 0.5, -0.14)	0	4	Climb

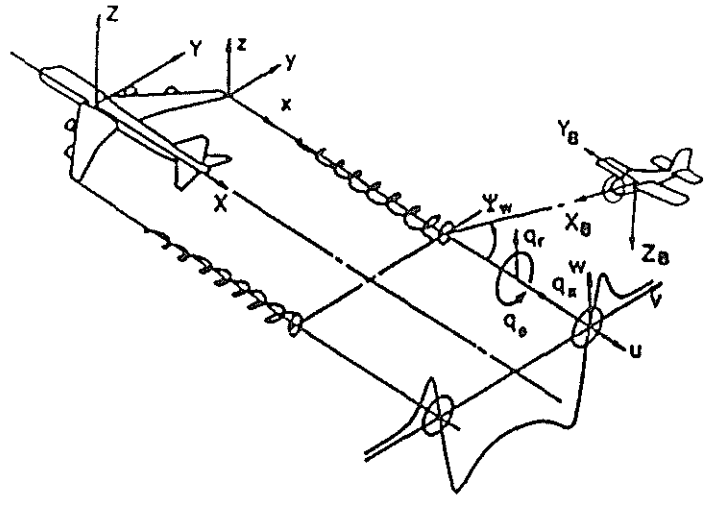

Figure 1. Geometrical relation among a preceding airplane, its trailing vortices and a penetrating aircraft.

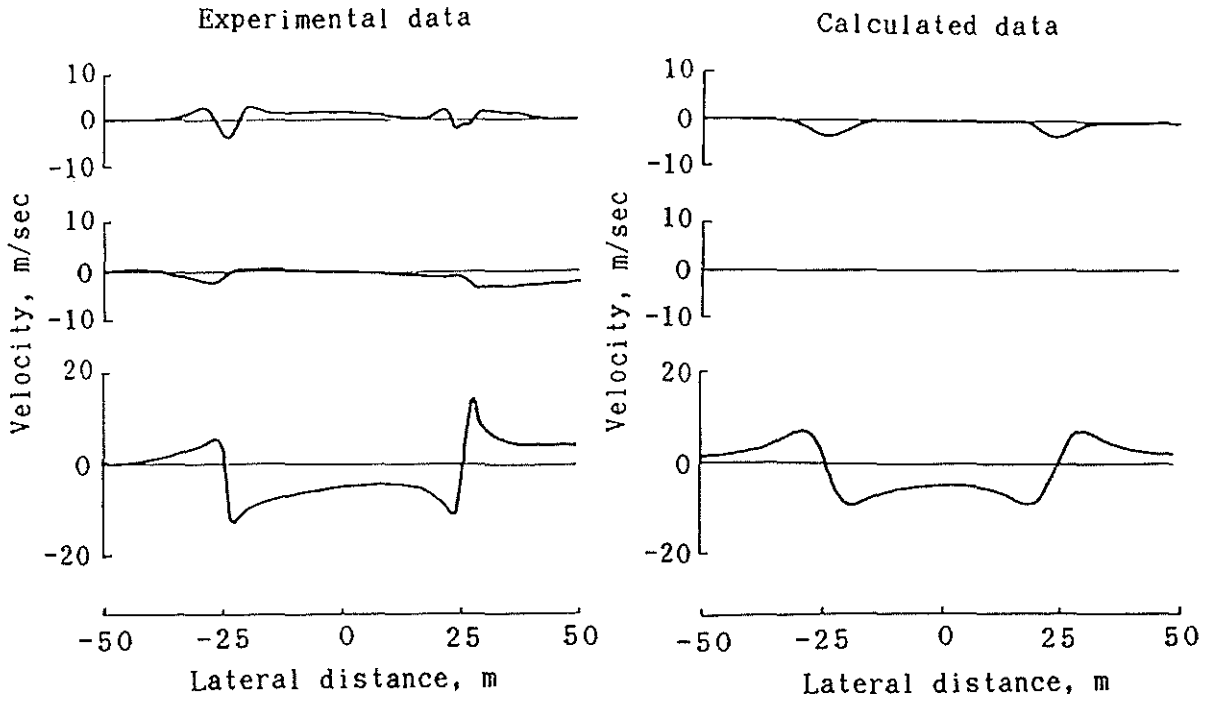

(a) Gust profile at separation distance of x=10,500 m

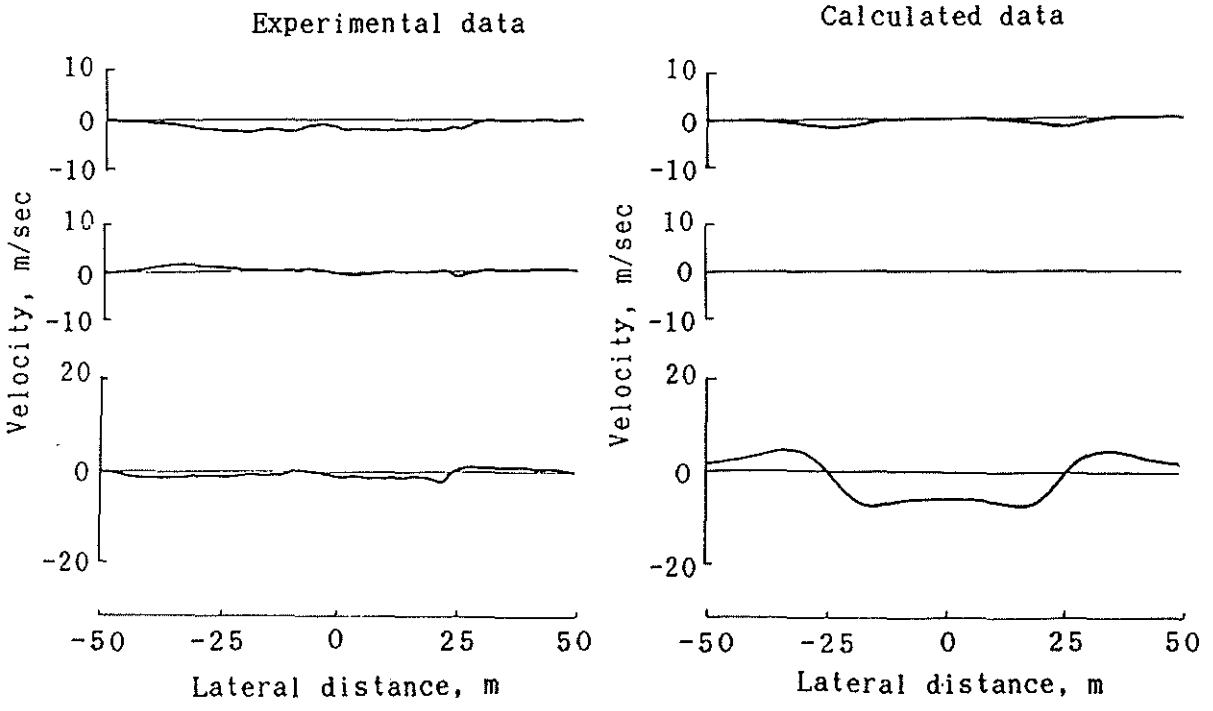

(b) Gust profile at separation distance of x=24,000 m

Figure 2. Comparison of calculated gust profile of airplane wake with the experimental data [8]. (Preceding airplane : Boeing 747)

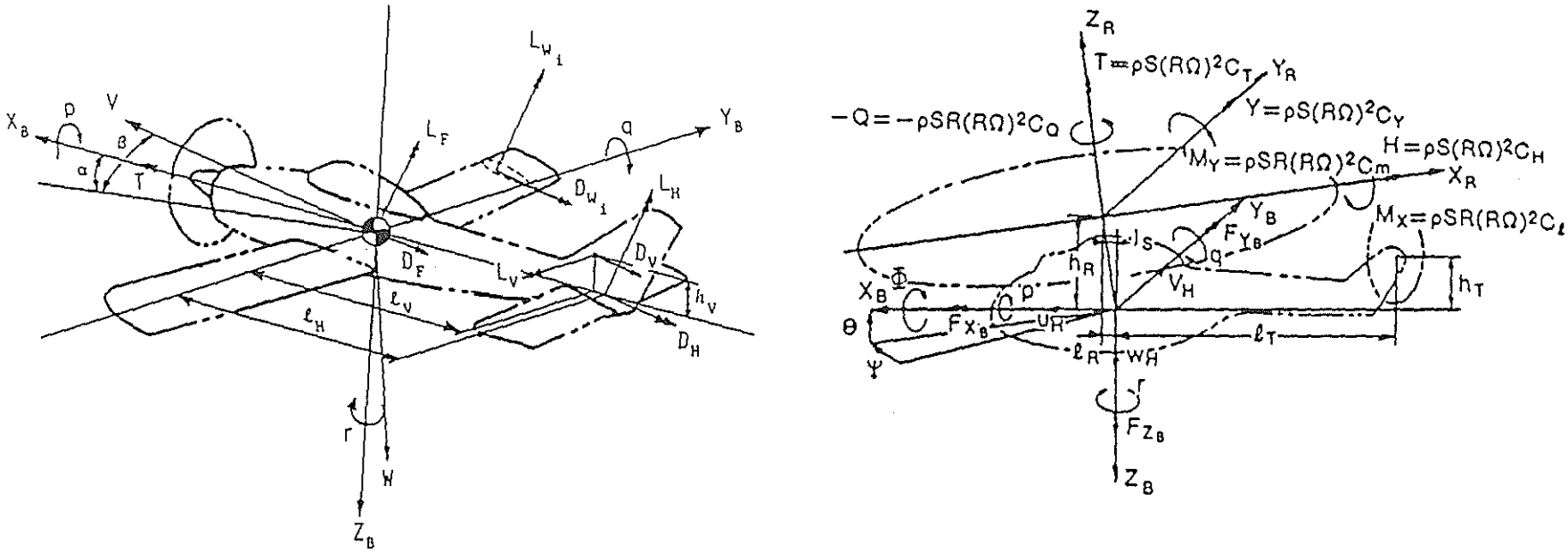

(a) Airplane

(b) Helicopter

Figure 3. Forces and moments acting on a penetrating aircraft.

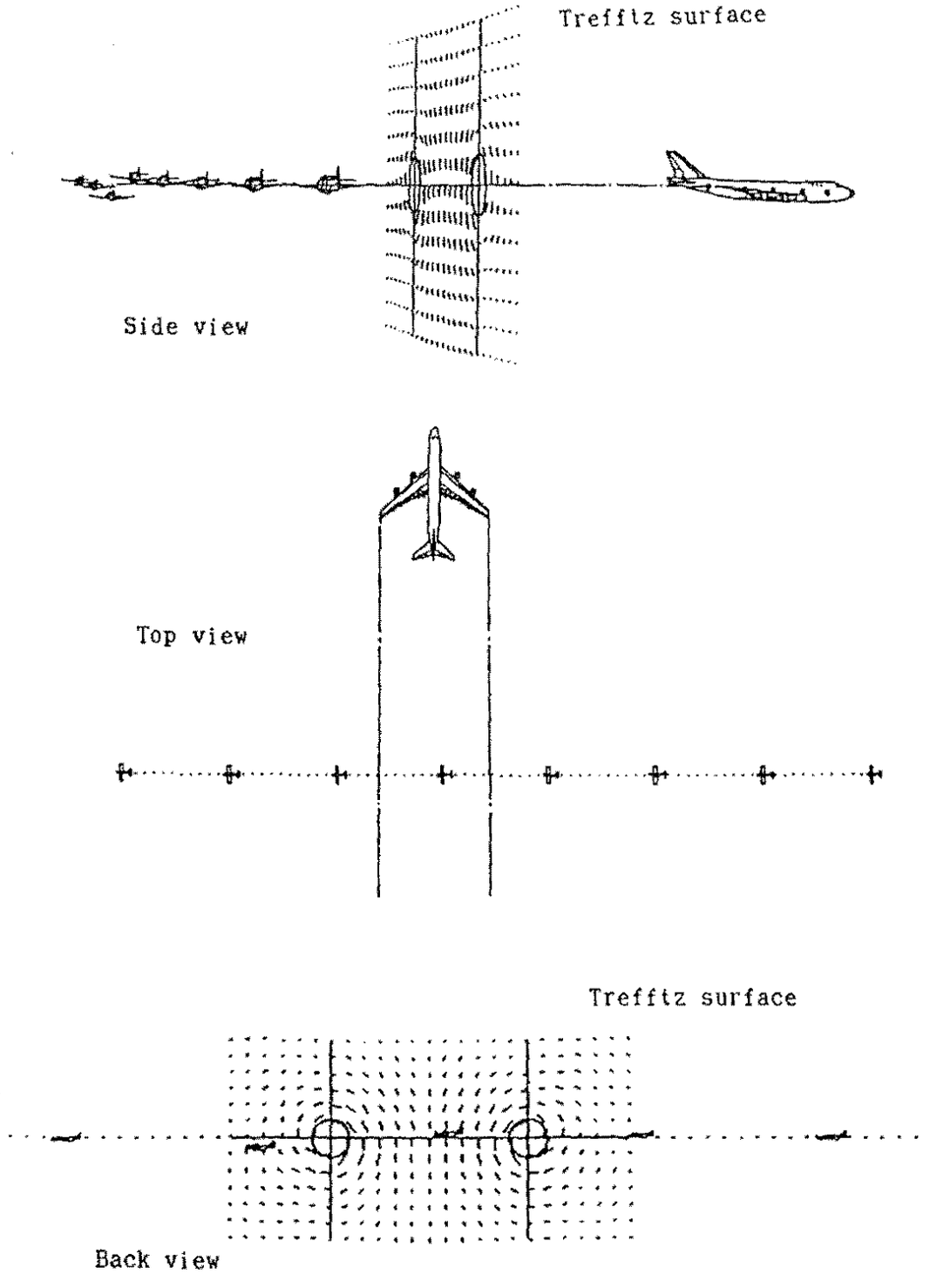

(a) For airplane

Figure 4. Typical example of the calculated flight trajectories. (Ψ_W=0 degree, γ=0 degree)

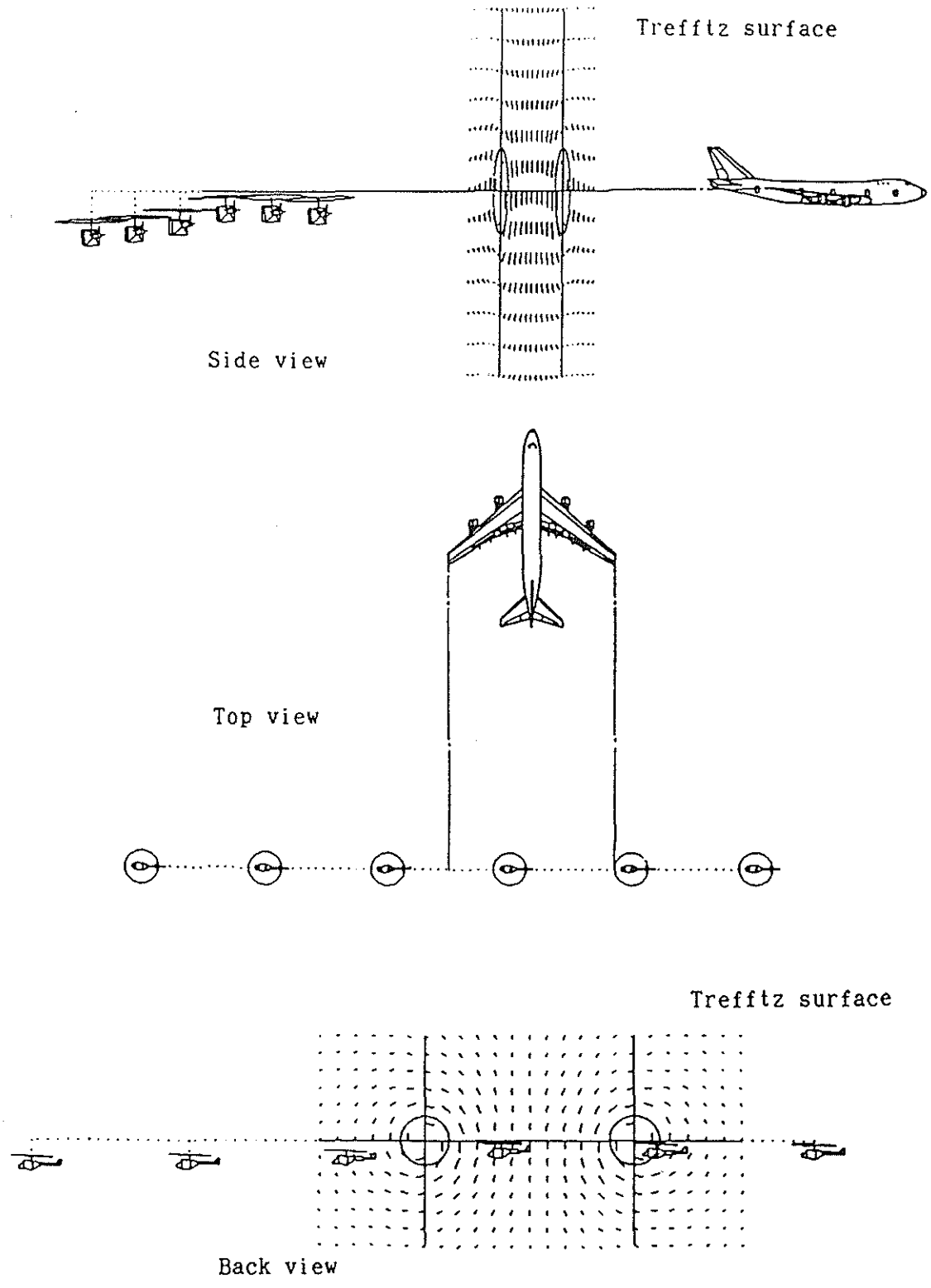

(b) For helicopter

Figure 4. - Concluded.

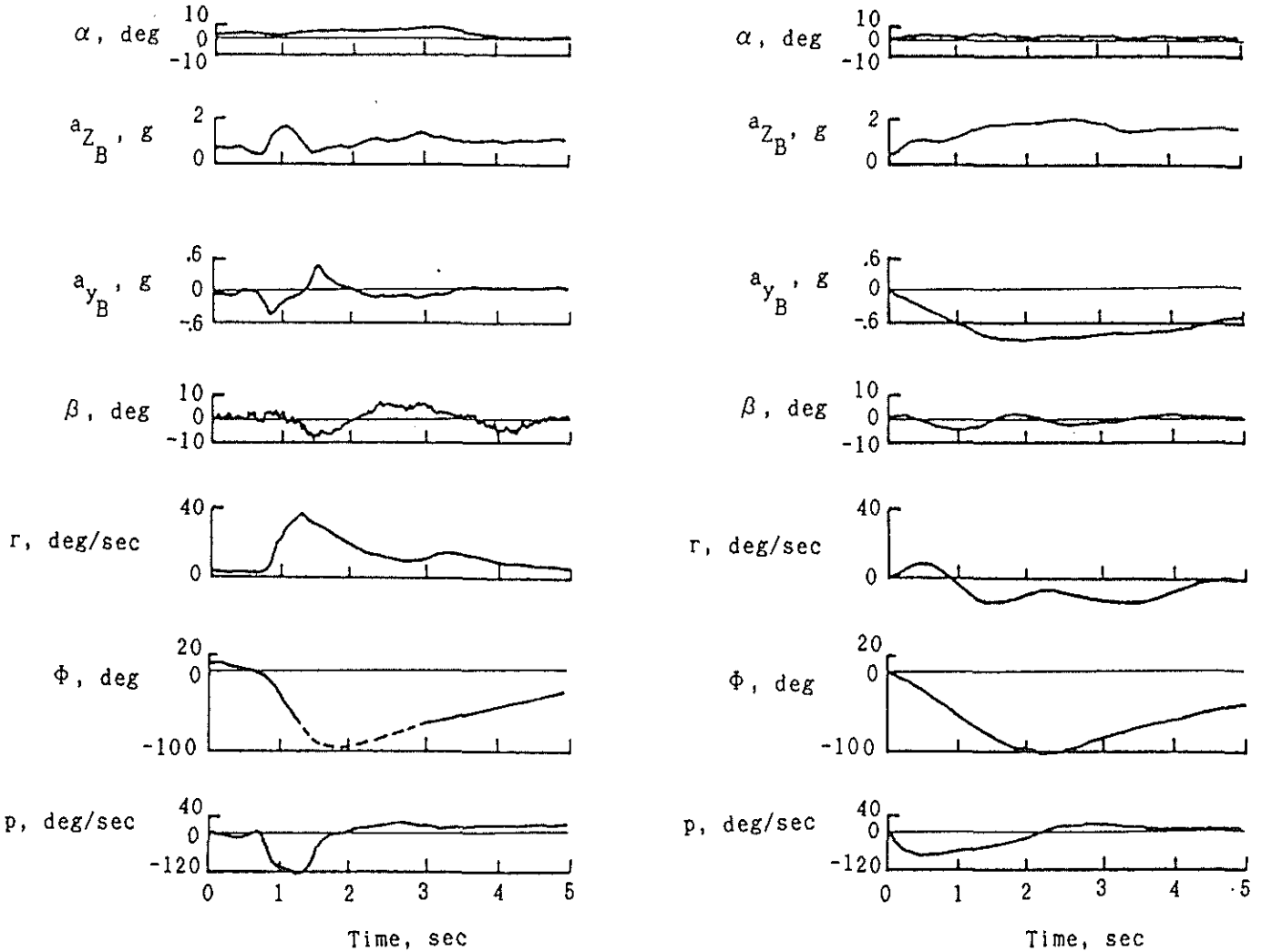

Flight test data

Calculated result (with aileron control)

Figure 5. Comparison of the calculated result of the dynamic response with the flight test data at separation distance of x=5,180 m [13]. (Preceding airplane : Convair 990, Penetrating airplane : Cassna 210)

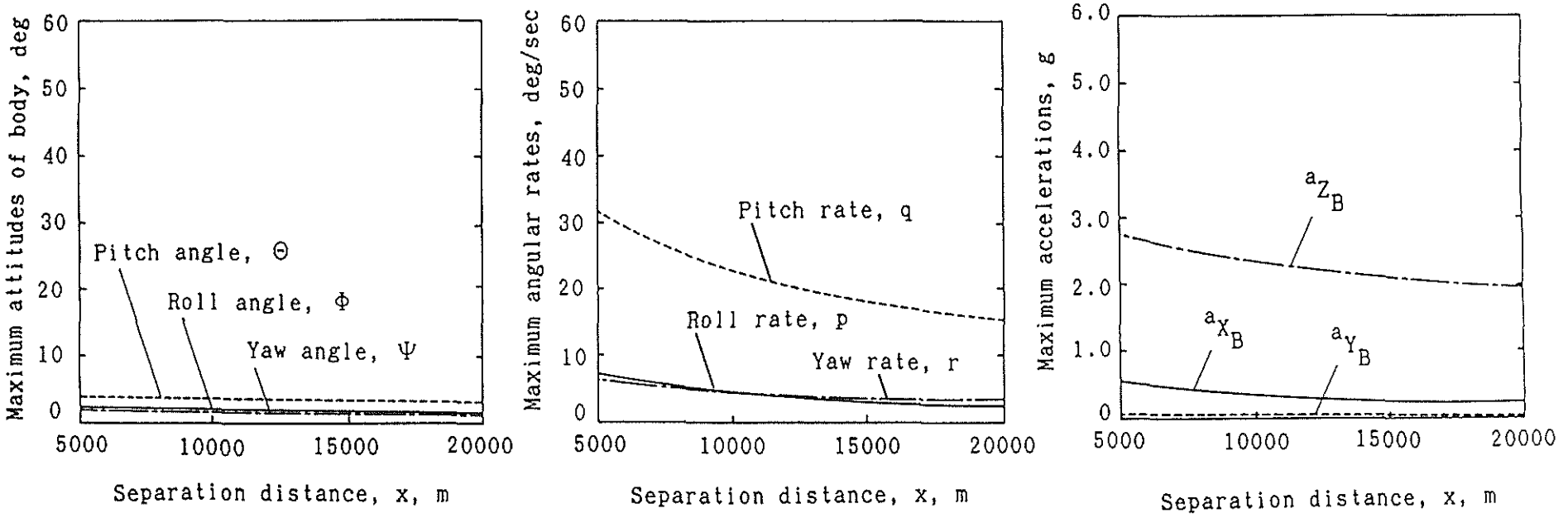

(a) For maximum attitudes, deg (b) For maximum angular rates, deg/sec (c) For maximum accelerations, g

Figure 6. Maximum dynamic response of the model A airplane against the separation distance. (Ψ_W=90 degrees, γ=0 degree)

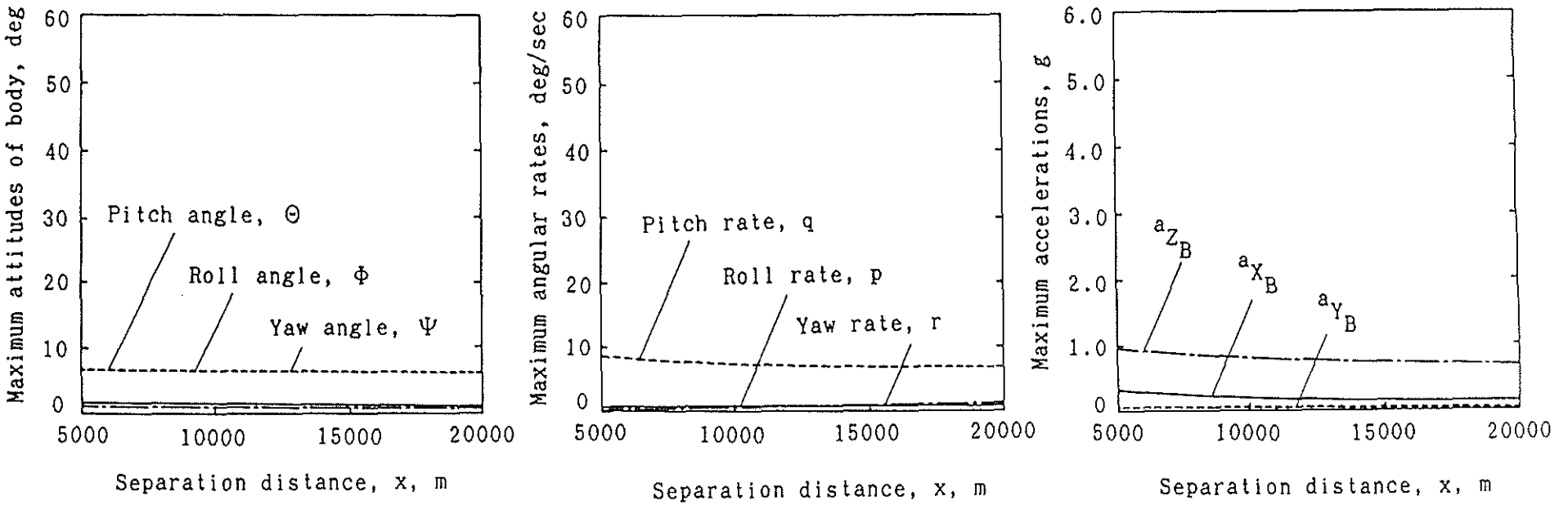

(a) For maximum attitudes, deg (b) For maximum angular rates, deg/sec (c) For maximum accelerations, g

Figure 7. Maximum dynamic response of the model B airplane against the separation distance. (Ψ_W=90 degrees, γ=0 degree)

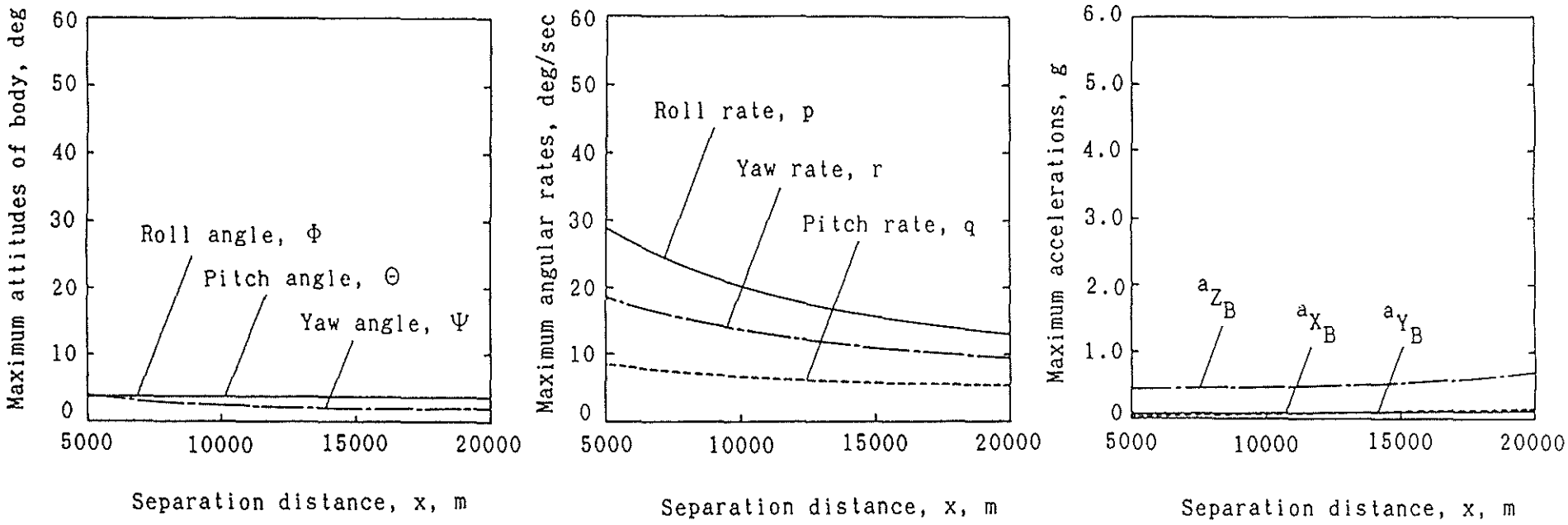

(a) For maximum attitudes, deg

(b) For maximum angular rates, deg/sec

(c) For maximum accelerations, g

Figure 8. Maximum dynamic response of the helicopter against the separation distance. (Ψ_W=90 degrees, γ=0 degree)

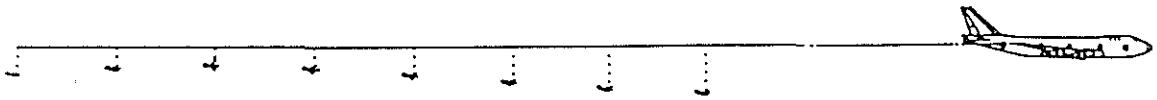

Side view

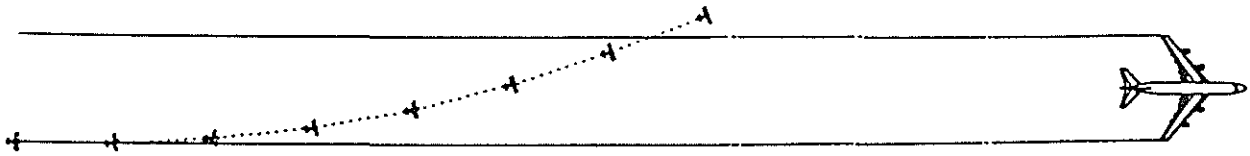

Top view

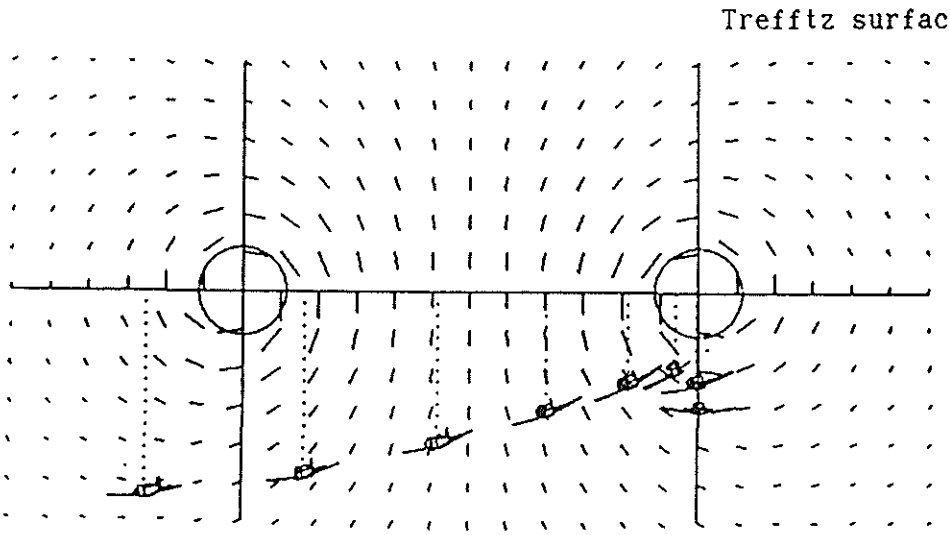

Back view

(a) For airplane

Figure 9 . Typical example of the calculated flight trajectories. (Ψ_W=0 degree, γ=4 degrees)

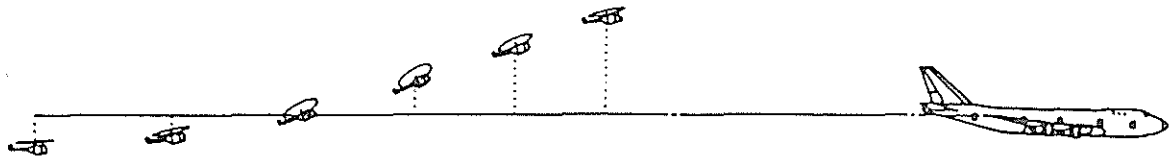

Side view

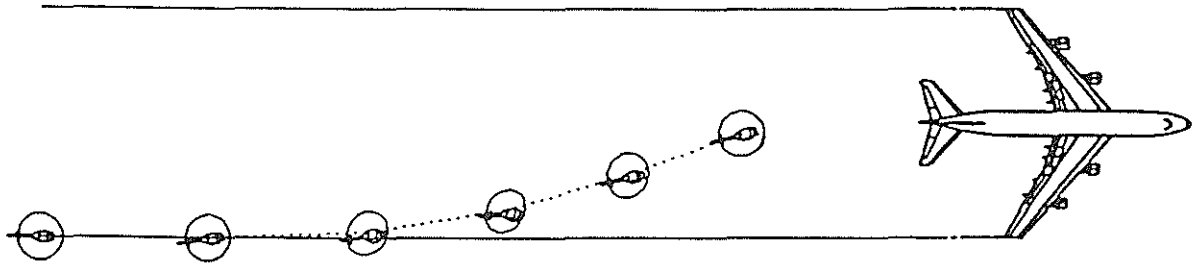

Top view

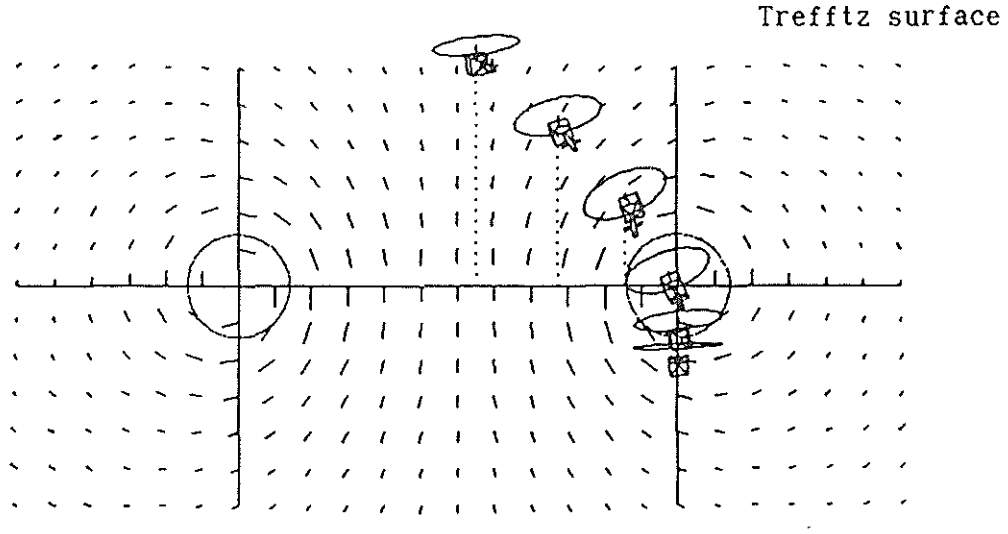

Back view

(b) For helicopter

Figure 9 . - Concluded.

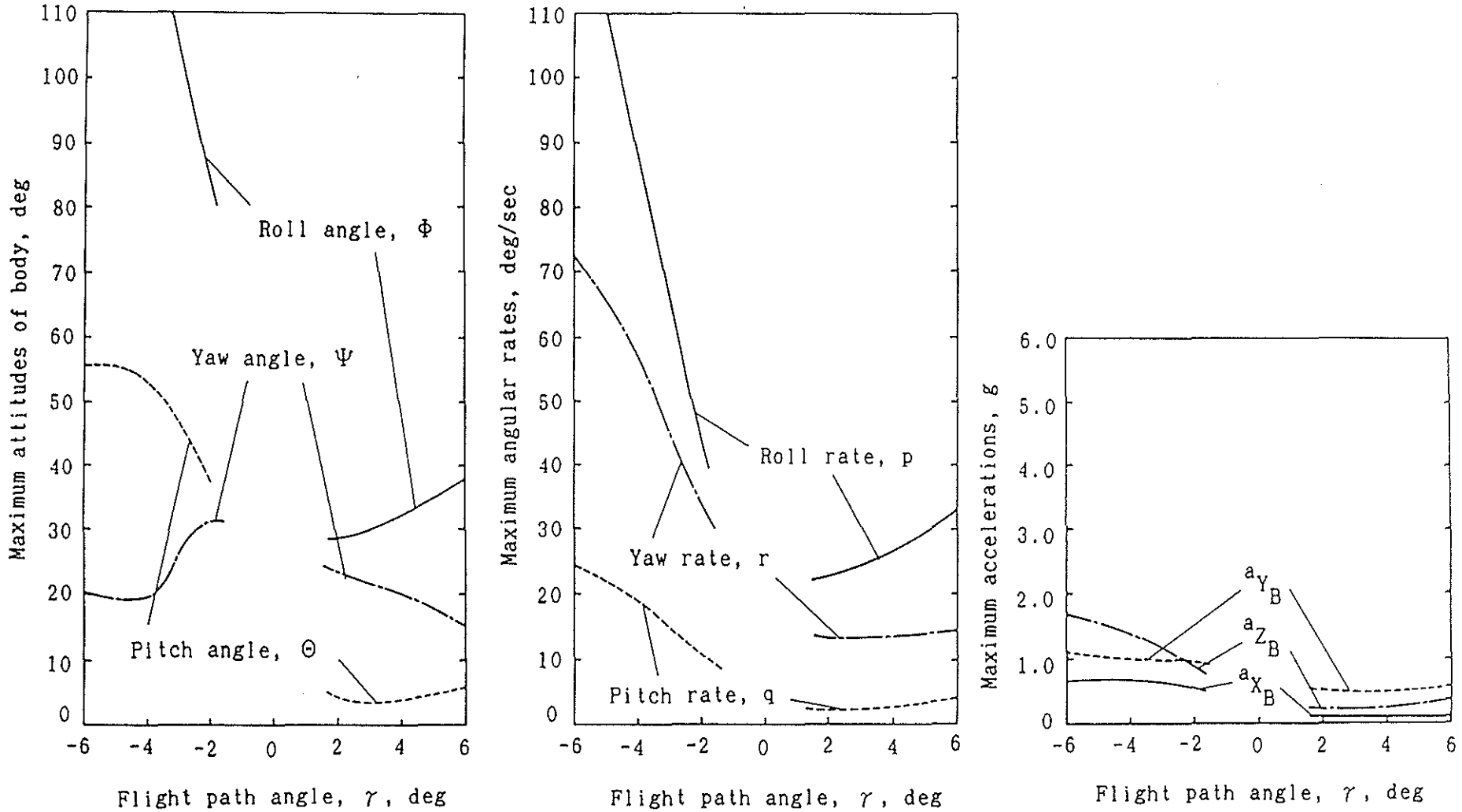

(a) For maximum attitudes, deg (b) For maximum angular rates, deg/sec (c) For maximum accelerations, g

Figure 10. Maximum dynamic response of the model A airplane against the flight path angle. (Ψ_W=0 degree, x=5,000 m)

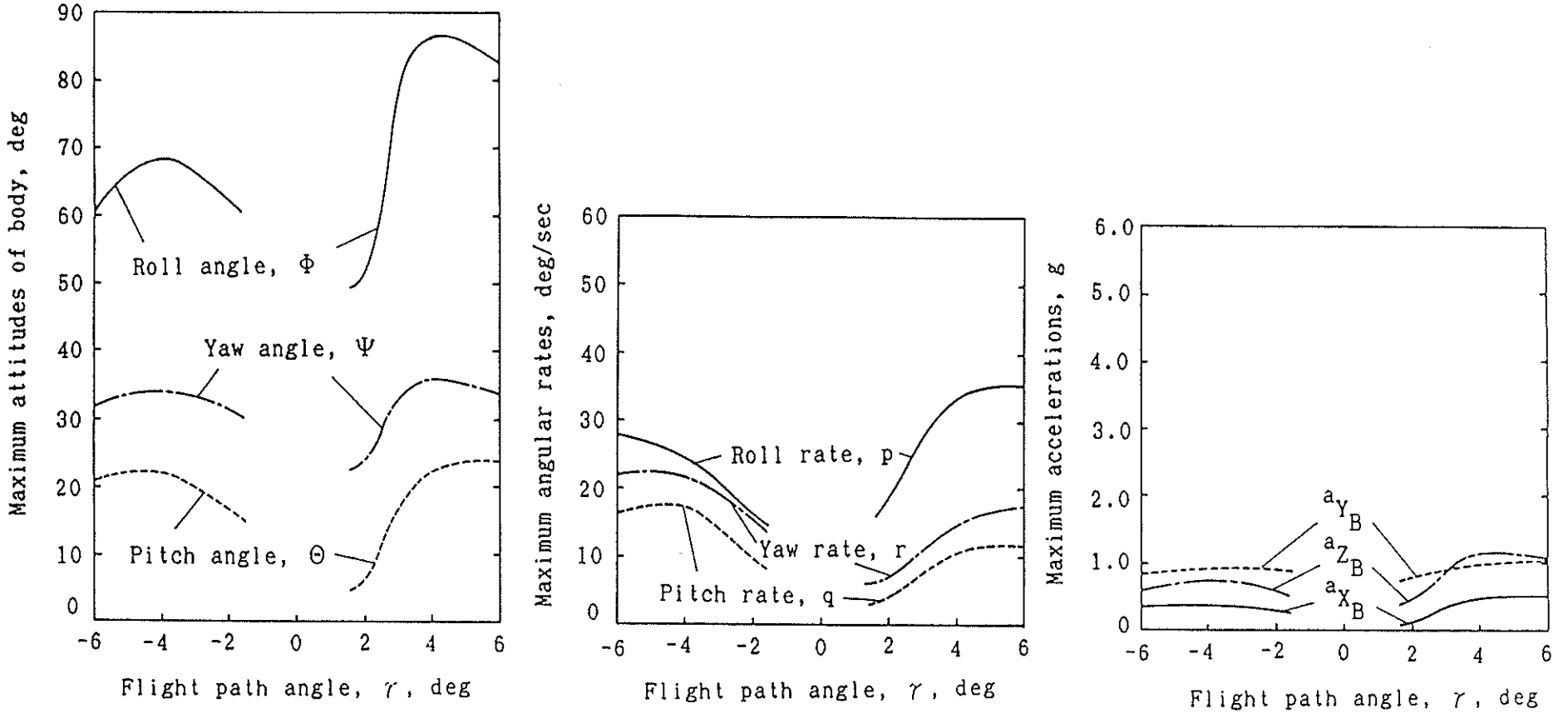

(a) For maximum attitudes, deg (b) For maximum angular rates, deg/sec (c) For maximum accelerations, g

Figure 11. Maximum dynamic response of the model B airplane against the flight path angle. (Ψ_W=0 degree, x=5,000 m)

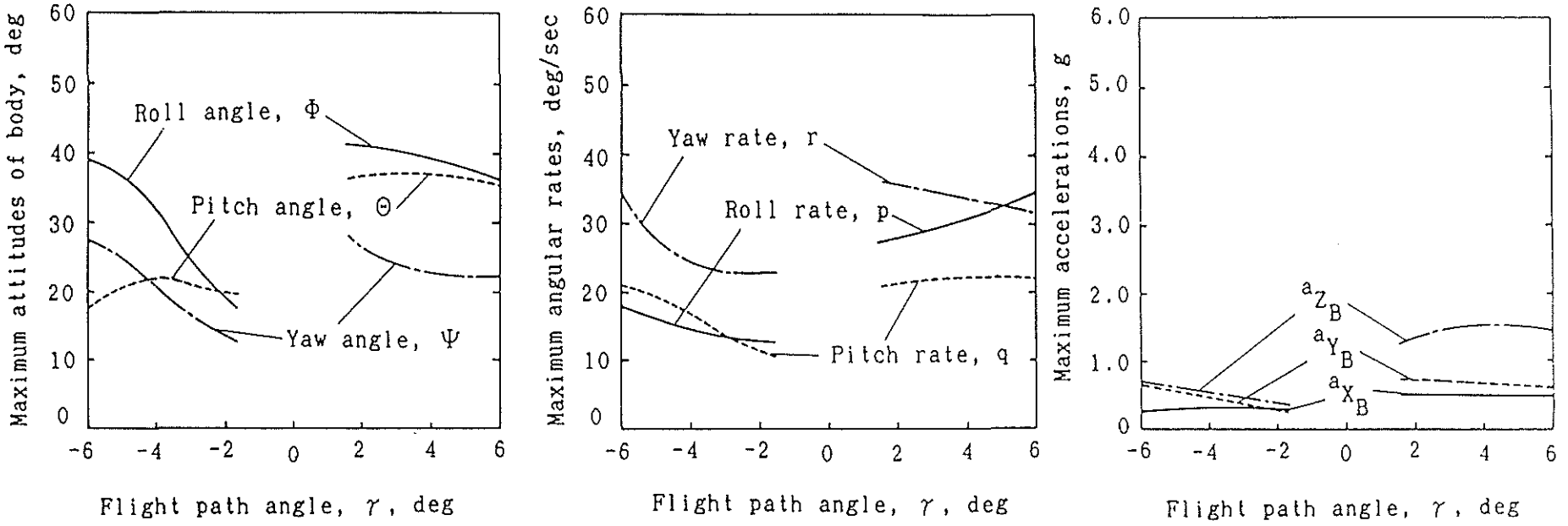

(a) For maximum attitudes, deg (b) For maximum angular rate, deg/sec (c) For maximum accelerations, g

Figure 12. Maximum dynamic response of the helicopter against the flight path angle. (Ψ_W=0 degree, x=5,000 m)

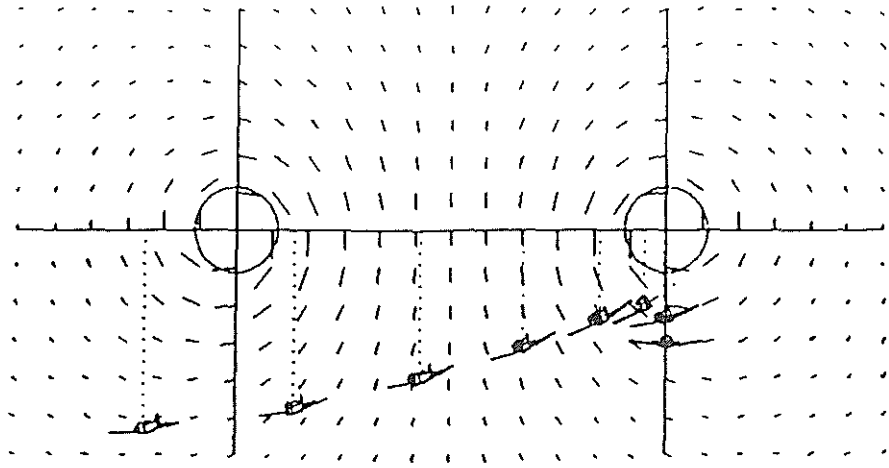

(a) For model A

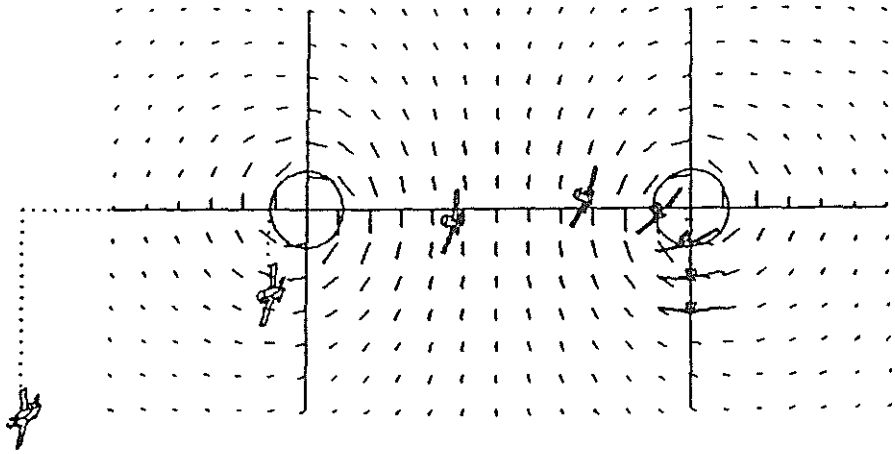

(b) For model B

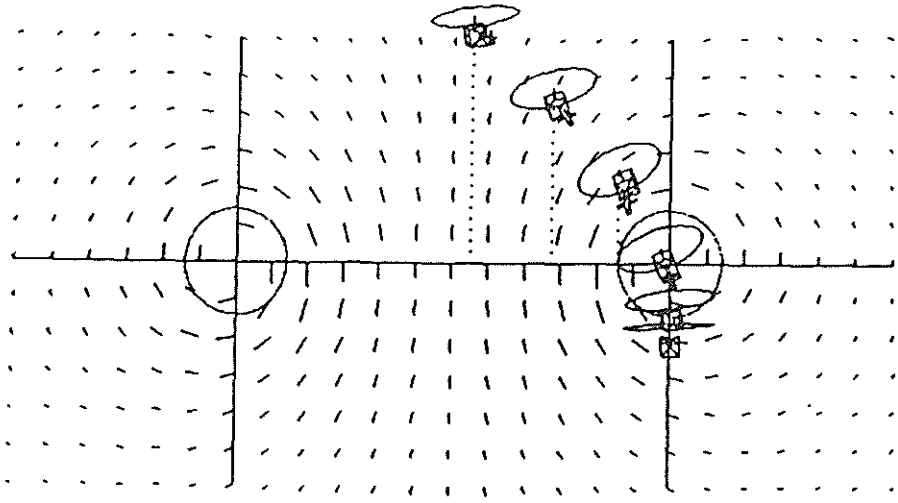

(c) For helicopter

Figure 13. Flight trajectories for three penetrating aircraft. (Ψ_W=0 degree, γ=4 degrees, x=10,000 m)

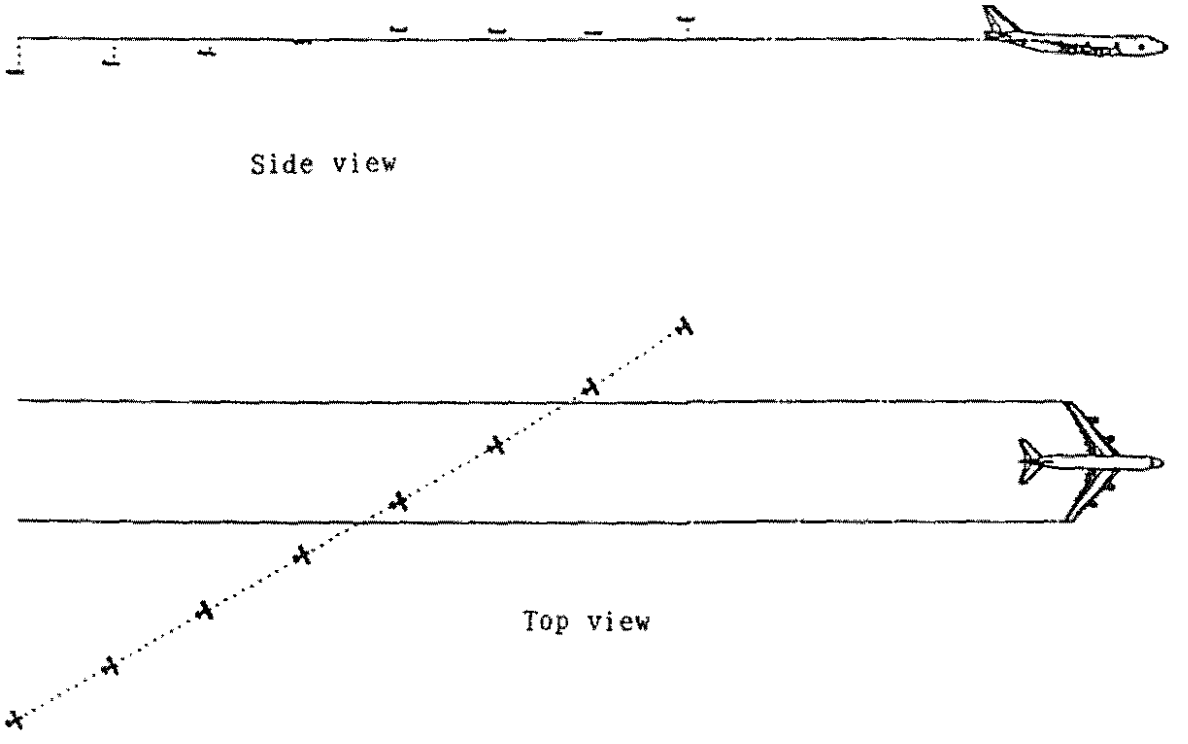

(a) For airplane

Figure 14. Typical example of the calculated flight trajectories. (Ψ_W=30 degrees, γ=5 degrees)

Side view

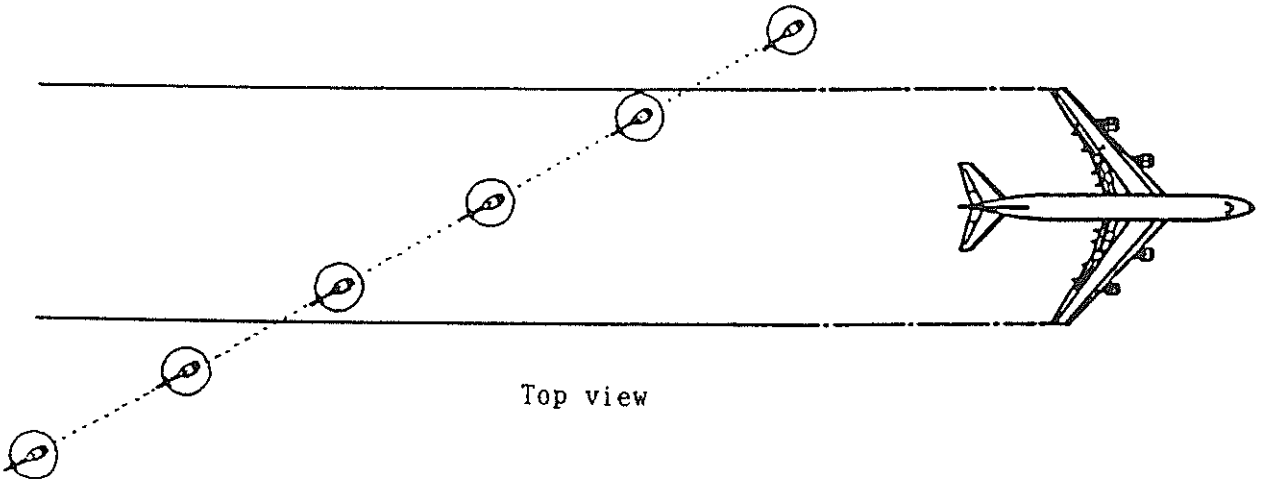

Top view

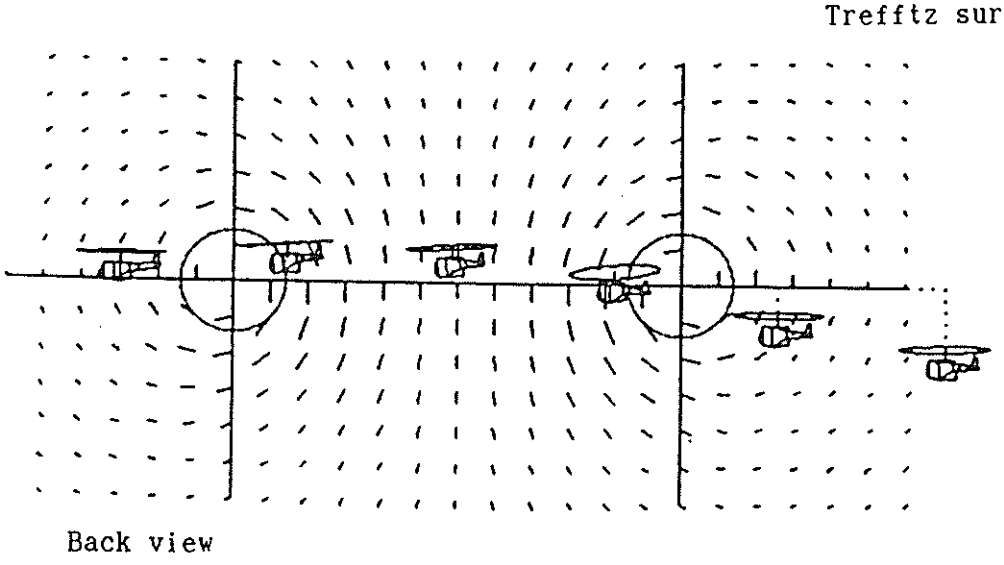

(b) For helicopter

Figure 14. - Concluded.

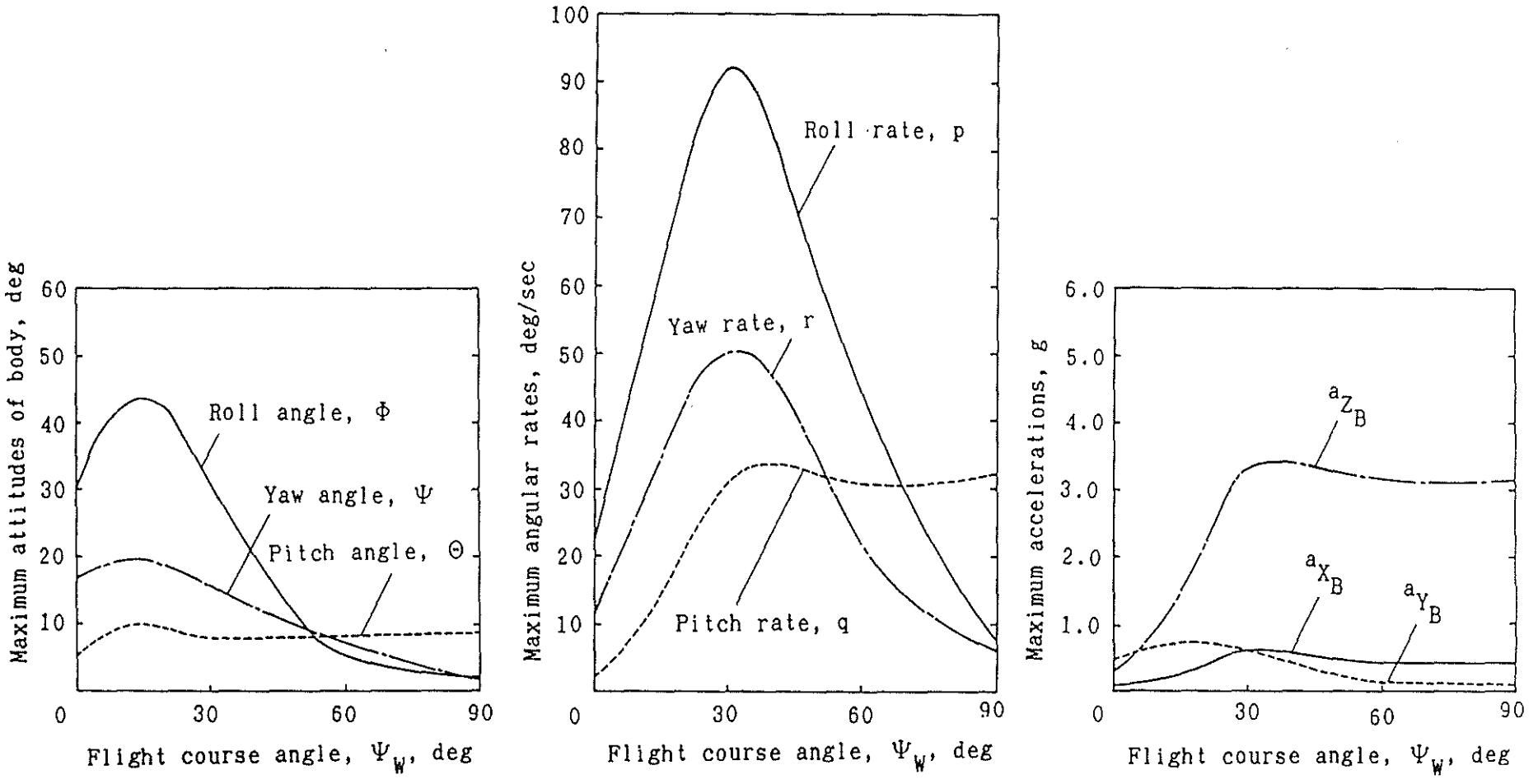

Figure 15. Maximum dynamic response of the model A airplane against the flight course angle. (γ=5 degrees, x=5,000 m)

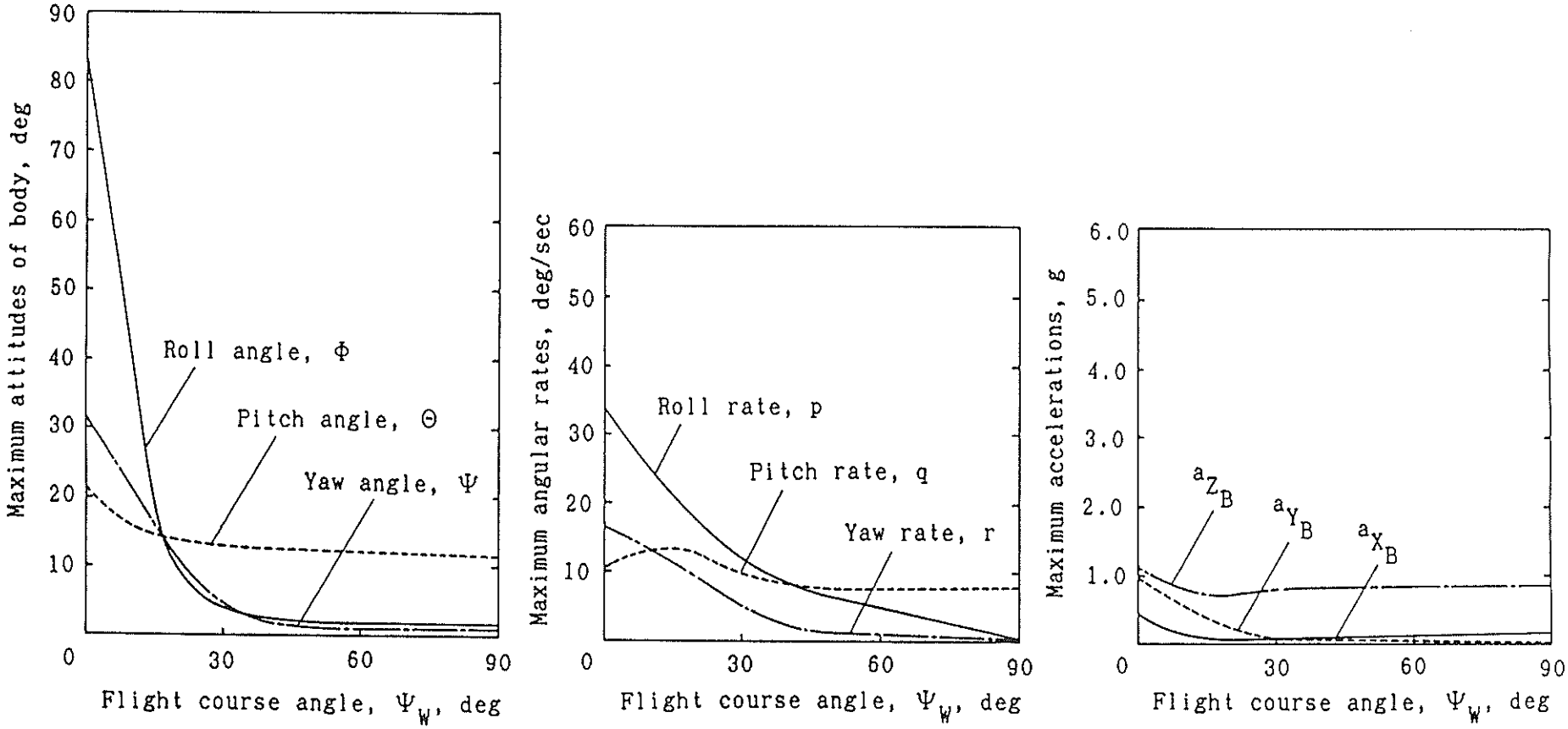

(a) For maximum attitudes, deg (b) For maximum angular rates, deg/sec (c) For maximum accelerations, g

Figure 16. Maximum dynamic response of the model B airplane against the flight course angle. (γ=5 degrees, x=5,000 m)

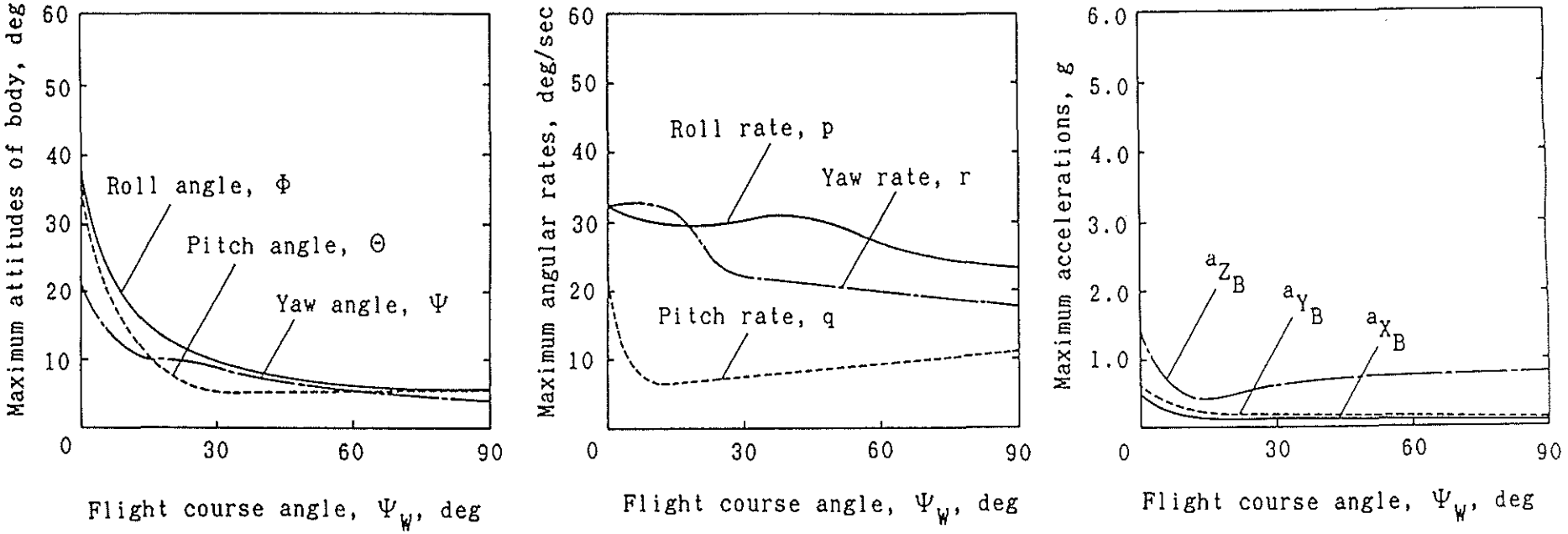

(a) For maximum attitudes, deg (b) For maximum angular rates, deg/sec (c) For maximum accelerations, g

Figure 17. Maximum dynamic response of the helicopter against the flight course angle. (γ=5 degrees, x=5,000 m)

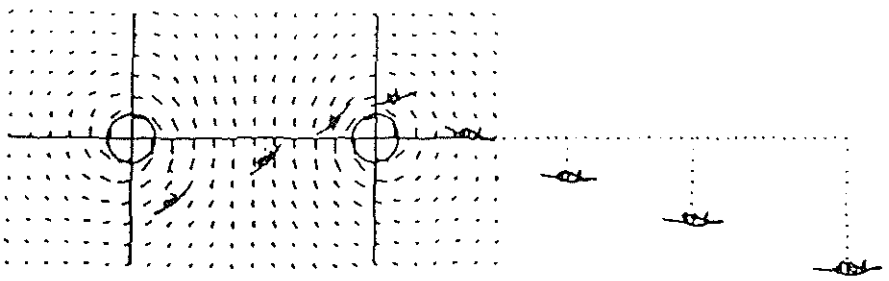

(a) For model A

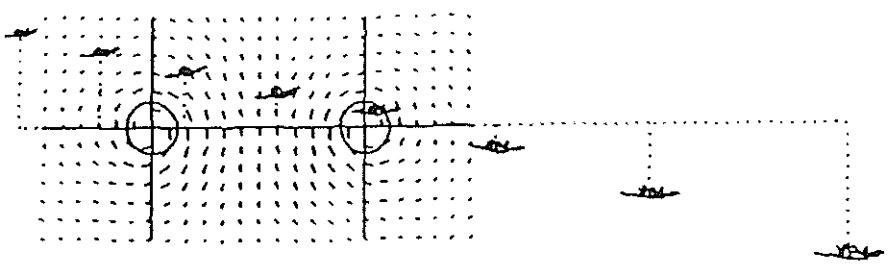

(b) For model B

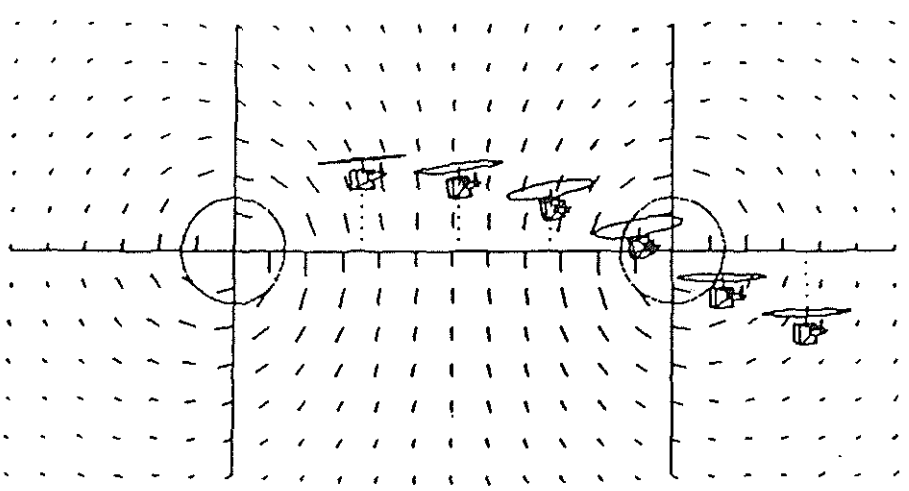

(c) For helicopter

Figure 18. Flight trajectories for three penetrating aircraft. (Ψ_W=30 degrees, γ=5 degrees, x=10,000 m)

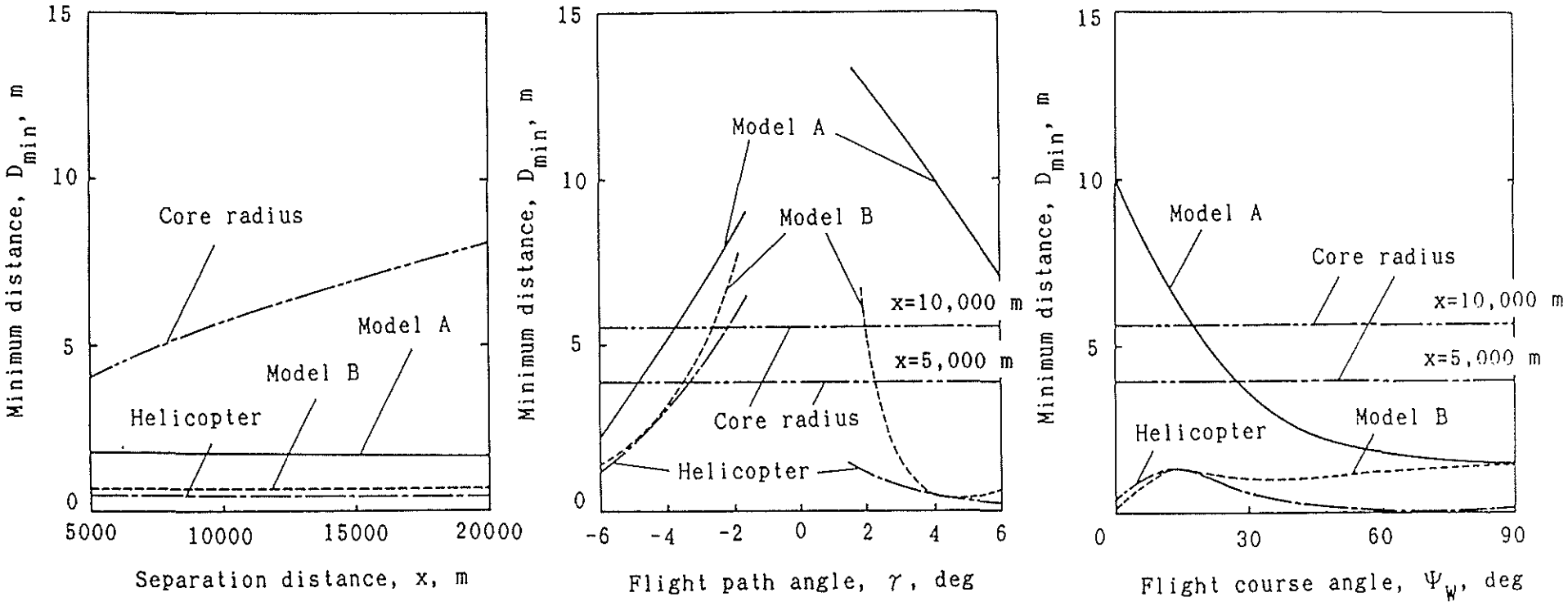

(a) For the separation distance (Ψ_W=90 degrees, γ=0 degree)

(b) For the flight path angle (Ψ_W=0 degree, x=5,000 m)

(c) For the flight course angle (γ=5 degrees, x=5,000 m

Figure 19. Minimum distance between the penetrating aircraft and the vortex core center.